Properties of localized, high latitude, dayside aurora

H. U. Frey,[1] T. J. Immel,[1] G. Lu,[2] J. Bonnell,[1] S. A. Fuselier,[3] S.B. Mende,[1] B. Hubert,[4] N. Østgaard,[1] G. Le[5]

Short title: LOCALIZED HIGH LATITUDE AURORA

Abstract. The FUV instrument on the IMAGE spacecraft frequently observes intense ultraviolet (UV) emission from a localized dayside region poleward of the general auroral oval location. One type of these emissions has been described as the signature of direct proton precipitation into the cusp after lobe reconnection during northward interplanetary magnetic field (IMF) and high solar wind dynamic pressure periods [*Frey et al.,* 2002]. Here we describe a completely different type of high latitude aurora, which does not show any signature of precipitating protons. It also occurs during northward IMF conditions however, only during periods of very low solar wind dynamic pressure. It occurs at a much higher geomagnetic latitude than the normal cusp location and only during periods of positive IMF B_y. The intensity of the UV emission is somewhat anti-correlated with the solar wind dynamic pressure, much in contrast to the cusp emission. Coincident measurements by the FAST spacecraft verify that this is not the cusp, that ion precipitation in these regions is absent, and that strong precipitation of field-aligned accelerated electrons causes the aurora. We interpret this aurora as the optical signature of electron precipitation in the upward leg of a current system which closes the downward leg of the current system into the cusp in the ionosphere.

1. Introduction

The objective of the IMAGE mission is to improve the understanding of magnetospheric processes and the interaction between solar wind, magnetosphere, and ionosphere. One signature of this interaction is the occurrence of aurora. The major objective of the Far Ultraviolet Instrument (FUV) on IMAGE is the observation of global changes in the aurora accompanying large-scale changes in the magnetosphere [*Mende et al.,* 2000].

In recent years, more attention has been given to the terrestrial aurora on the dayside and at high latitudes, as these regions tend to be more directly influenced by the solar wind and processes in the far magnetotail. The development of space-based UV-imagers has enabled year-round observations which can now be compared to in-situ measurements in the solar wind or magnetosphere.

Many different types of localized aurora at high latitude in the polar cap have been described. Polar-cap patches occur predominantly during southward IMF, show enhanced optical red-line emission from soft particle precipitation, and drift in the anti-sunward direction (see e.g. [*Walker et al.,* 1999]). Poleward moving auroral forms appear pre-noon and post-noon during primarily southward IMF [*Fasel,* 1995]. They are long (in MLT) and thin (in latitude) auroral arcs, which separate from the dayside auroral oval, move poleward for several minutes, and disappear inside the polar cap [*Drury et al.,* 2002]. Their average lifetime is of the order of 10 minutes and is explained with pulsed reconnection [*Sandholt and Farrugia,* 1999]. Many different kinds of arc-like features in the polar cap have been reviewed and summarized by *Zhu et al.,* [1997]. These features appear during northward IMF conditions and are described as sun-aligned arcs, transpolar arcs, or theta-aurora. They appear mostly during quiet geomagnetic conditions. The occurrence of polar cap arcs with respect to IMF B_y showed arcs in the dusk sector for positive B_y and in the dawn sector for negative B_y, respectively [*Elphinstone et al.,* 1990].

Large-scale dayside auroral features were described by *Murphree et al.,* [1990] during periods of northward IMF with IMF B_x <0 and B_y >0. The fact that during several of their observations transpolar arcs were connected to these localized emission regions let them conclude that they originated at the high latitude magnetopause, poleward of the cusp. In a later paper *Elphinstone et al.* [1993] summarized the dayside auroral features seen by the UV imager on Viking and demonstrated the relation of westward and anti-sunward motion of high latitude dayside auroral forms with anti-parallel merging at the front side magnetotail.

Ohtani et al. [1997] extended an earlier investigation of dayside aurora by *Murphree and Elphinstone* [1988] with IMF, ground magnetometer and DMSP satellite particle data and showed the response to changes in the IMF. The solar wind density and velocity were constant, and the appearance of an auroral spot in the afternoon sector was explained by a sudden increase of the IMF B_z.

Another high latitude, dayside region of aurora is the cusp [*Smith and Lockwood,* 1996]. Auroral forms in the cusp were described from ground-based meridian scanning photometer and all-sky camera observations [*Sandholt et al.,* 1998]. The location of the Svalbard ground site at 75° magnetic latitude enabled studies during northern winter months between 70-80° latitude and the relative motion of the site allowed for the study of the local time dependence on the IMF east-west B_y component. They demonstrated the dependence of the cusp location on the IMF, with lower latitudes for negative, and higher latitudes for positive B_z.

Milan et al. [2000] described an event study of an interval of northward IMF, where they observed cusp aurora near local noon poleward of the dayside auroral oval with the UVI instrument on the Polar satellite. They interpreted this emission as the signature of high latitude reconnection and described its motion in response to IMF B_y changes.

These investigations were recently extended with results from the FUV instrument on IMAGE, which is capable of distinguishing between proton and electron produced

aurora. In a statistical study, *Frey et al.* [2002] demonstrated the dependence of the proton aurora intensity in the cusp on the solar wind dynamic pressure. They also showed the dependence of the cusp location on IMF B_y. Furthermore, the dependence of the latitude location on B_z was demonstrated [*Fuselier et al.,* 2002].

In this paper we perform a statistical analysis of a different kind of high latitude aurora, which lacks any proton contribution. We correlate the aurora emission at high latitudes as observed by the IMAGE-FUV instrument with the corresponding solar wind parameters, and give an explanation of their physical nature. After a brief summary of instrumentation and analysis techniques we discuss individual observations and conclude with the statistical study of 13 cases.

2. Instrumentation and data analysis

The IMAGE satellite is in a highly elliptical orbit of 1000 x 45600 km altitude. The Far Ultra-Violet imager (FUV) consists of three imaging sub-instruments and observes the aurora for 5-10 seconds during every 2 minute spin period [*Mende et al.,* 2000]. Major properties such as fields of view, spatial resolution and spectral sensitivity were validated by in-flight calibrations with stars [*Gladstone et al.,* 2001]. The Wideband Imaging Camera (WIC) has a passband of 140-180 nm. It measures emissions from the N_2 LBH-band and atomic NI lines, with small contributions from the OI 135.6 nm line. The proton aurora imaging Spectrographic Imager channel (SI-12) is sensitive to the Doppler-shifted Lyman-α emission around 121.8 nm from charge-exchanging precipitating protons. The instrument properties do not allow determination of the exact Doppler shift and the energy of the emitting hydrogen atom. However, as was confirmed by theoretical modeling, it is mostly sensitive to proton precipitation in the energy range of 2-8 keV, with very low sensitivity below 1 keV [*Gérard et al.,* 2000, 2001]. The oxygen imaging Spectrographic Imager channel (SI-13) has a passband of 5 nm around the 135.6 nm doublet of oxygen OI emission. The measured signal is

a combination of OI and some contribution from lines in the N_2 LBH emission band (20-50 % depending on electron energy).

Solar wind parameters for this study were obtained through CDAWeb from the Wind and Geotail spacecraft. The Geotail apogee of 30 Earth radii was located at about 2000 local time. Measurements within the magnetosphere were discarded for this study. Wind changed position from a location at 260 R_e at 0600 local time to 120 R_e at 0900 local time. All solar wind properties were propagated to Earth using the instantaneous solar wind speed values.

During the time period of April 24 to June 19, 2001 (days of year 114-170) 13 clear cases and 73 hours total of a localized bright UV emission on the dayside were found (Table 1). Figure 1 shows examples from four different days, when the localized feature could be observed with WIC poleward of the dayside auroral oval location. For a comparison we also show the corresponding SI-12 images, which do not show any signature of energetic proton precipitation. The three selection criteria for the events were:

Table 1

Figure 1

- A localized region of bright emission had to be found poleward of the auroral oval in the WIC images.
- The localized region had to be observable for at least 20 minutes.
- No signature is allowed in the SI-12 images.

The third criterion eliminated several time periods of proton precipitation into the cusp similar to those previously described by *Frey et al.,* [2002]. Each individual time sequence of WIC images was then analyzed in the following manner. Whenever the bright feature was seen, the mean count rate in a region of 5x5 pixels (about 250x250 km from apogee) around the brightest pixel was determined, as well as the location in magnetic local time (MLT) and geomagnetic latitude. The SI-13 and SI-12 instrument

responses were then determined for the same location. If the instrument response of WIC to the localized emission dropped below background level, the last location was tracked for another 30 minutes. If the emission appeared again within 30 minutes, the whole sequence was considered a continuous event. If the emission did not appear again, data for 15 minutes of observations following the disappearance were still included in this study.

3. FUV observations

3.1. April 28, 2001

FUV observations on April 28, 2001 (doy=118) show the most dramatic increase in WIC signal (Figure 2). Around 21:00 UT no signal above the dayglow could be seen. The time-propagated solar wind density was about 4 cm^{-3} before 20:45 when it dropped to values below 2 cm^{-3} and stayed there for another hour (Figure 3). All three IMF components were positive during the whole time period. The first sign of an increased localized dayside emission could be seen in the image from 21:12. Within 8 minutes the brightness increased by a factor of 7 and remained bright after 21:20 until FUV was turned off for entry into the radiation belt at 21:33. During the whole time period no change in SI-12 signal aside from statistical background fluctuations were observed in the corresponding region. SI-13, which is also sensitive to FUV emission from electron precipitation, showed a similar increase in response as WIC. No obvious change in the solar wind properties could be related to the start of the brightness increase. The 8 minutes time difference between the propagated Wind and Geotail measurements (top panel in Figure 3) show the approximate propagation uncertainty. However, the time difference between the drop in density and the increase in emission was much larger than this propagation uncertainty.

Figure 2

Figure 3

3.2. May 25, 2001

FUV observations on May 25, 2001 (doy=145) show a long lasting localized emission (Figure 4). During the entire period of observations the solar wind density stayed between 1-2 cm^{-3} (Figure 5). The IMF B_z changed between -2 and +2 nT and B_x and B_y stayed negative and positive, respectively. After a period of rather constant but dim emissions, the spot-like region underwent repeated increases and decreases in brightness between 08:30 and 14:30. The time differences between brightness maxima decreased with time from 70 minutes to 30 minutes. The location of the brightest emission changed slowly with time from 77° to 83° latitude. The MLT location changed too, from 1300 during low values of IMF B_y (0500 UT) to 1600 later at 1100 UT when B_y had increased to 6 nT. During the whole time period, the only variations in the proton imager's response were small statistical fluctuations.

Figure 4

Figure 5

3.3. May 25/26, 2001

The observations on May 25/26, 2001 (doy=145/146) are summarized in Figure 6. This represents a time period with mostly positive IMF B_x conditions. The observations coincided with a simultaneous FAST pass through the region of localized emission. Figure 7 shows the WIC image taken at 01:17:13 with the footpoints of FAST from one minute before to 3 minutes after the image integration. The FAST location is indicated by the small asterisk. This image is obtained just prior to the FAST passage through the bright spot, which is located at 83° latitude and 12:50 MLT. The FAST measurements are summarized in Figure 8. The magnetic field disturbance in the cross-track direction (green line, top panel) shows two major field-aligned current regions. The more equatorward region of measurements between 01:15:50 and 01:17:10 (positive slope) shows a downward current region which coincides with the 0.1-2 keV ion and very low electron energy (<500 eV) cusp precipitation. Poleward of this, there is an upward current region (01:17:10-01:20:00, negative slope) without any proton

Figure 6

Figure 7

Figure 8

precipitation, and a signature of latitude-energy dispersed electron precipitation and inverted-V like structures after 0118 UT. In the dayside region of 84.5-86.8° latitude along the 1230 MLT meridian, this inverted-V like structure is quite unusual.

An analysis of the FAST measurements indicates, that the electrons are likely to come from closed, and not from open field lines. Spectra of electrons from open field lines show electron source temperatures of a few tens of eV, as for instance around 0117 UT in the cusp (Figure 8). The electrons at higher latitude (01:19:30 UT) have an electron source temperature of 300-400 eV, which indicates a source in the plasma sheet.

3.4. May 24, 2001

The observations on May 24, 2001 (doy=144) are summarized in Figure 9. With the exception of two very short intervals, the IMF B_x was always negative. B_z was almost always northward, but with small values of 0-4 nT. B_y was the largest component with always positive values between 3-8 nT. As in the previous cases, WIC showed several periods of increased brightness from electron precipitation, while the proton imager does not show any strong signals.

Figure 9

This time interval coincided with a FAST pass through the localized region of strong electron precipitation (Figure 10), which is summarized in Figure 11. The lower latitude cusp-like precipitation region was traversed between 18:42:00 and 18:43:30 (78.4-80.7° magnetic latitude). This is the region of downward field-aligned current, medium energy ion precipitation, and electron energies below 500 eV. The region of downward field-aligned current at higher latitudes shows a strong electron energy-latitude dispersion, with the highest energies of 10 keV at 83.7° latitude. This region is practically void of ion precipitation, and the measurements show an inverted-V electron spectrum.

Figure 10

Figure 11

A mapping code was developed which maps any location in an FUV-image into the magnetosphere [*Fuselier et al.,* 2001b]. It uses external solar wind parameters (IMF,

pressure) and the Tsyganenko magnetic field model [*Tsyganenko,* 1995; *Tsyganenko and Stern,* 1996]. Figure 12 shows the mapping of six points along the perimeter of the bright electron-produced emission in the 18:46:39 image, and additionally two points from the dark region of downward current are mapped too. The low solar wind dynamic pressure of 0.4 nPa allowed the magnetopause to move outward to about 15 R_e. At this time the B_x component was negative, and the positive IMF y- and z-components would favor anti-parallel reconnection at the high latitude, duskside magnetopause. The fieldlines from the spot map into this direction however, they do not come close enough to the magnetopause to allow for a reconnection with the draped fieldlines in the magnetosheath. Rather, they map into the distant tail. Furthermore, the IMF orientation is not consistent with the anti-parallel reconnection to these field lines, as the angle between the IMF and the magnetospheric field lines from the spot would be $\approx 140°$ and not 180°. The two field lines from the dark region of downward current map close to the high latitude magnetopause where they may be able to reconnect to the solar wind magnetic field.

Figure 12

4. Statistical summary

4.1. Location of emission

All examples of bright, localized electron aurora were found to occur between 73° and 89° geomagnetic latitude with mean and median values of 82.4° and 82.9°, respectively (Figure 13). Their locations were distributed between 7.9 and 19.9 hours MLT, and the median and mean MLT have the same values of 14.6 hours.

Figure 13

Although the distribution of these locations resembles general features of the proton aurora in the cusp observations [*Frey et al.,* 2002], they are different in the mean values. The mean latitude location is 3° higher compared to the mean cusp proton latitude of 79.2°. The local time of this localized emission is almost 3 hours later compared to the

11.7 hours location of the proton cusp. Later we will show that these differences are not caused by a bias of the data sampling, but rather are a true characteristics of this phenomenon.

4.2. Dependence of emission on solar wind magnetic field

The propagated solar wind measurements were used to determine the correlation between the location and intensity of the localized emission, and the solar wind magnetic field and plasma parameters. The relationship between the IMF GSM B_z value and the location and FUV emission is given in Figure 14. Observations were performed during periods when B_z was between -6 nT and 12 nT, but there does not seem to be a clear dependence of the latitude location on B_z. The intensity of the FUV emission is not biased towards specific values of B_z, as the correlation coefficient reaches only -0.13. Figure 14

Figure 15 summarizes the dependence of the magnetic local time location and WIC signal on the value of IMF B_y. As we did not find any time period with negative B_y values, there are only measurements in the positive range of B_y. There is a trend towards later local times with increasing B_y, though the correlation coefficient reaches only 0.33. As almost all observations were performed during steady IMF B_y conditions, we can not determine any temporal dependence of the MLT location with changes in B_y. Figure 15

Most observations reported here were made during negative IMF B_x conditions (Figure 16). The minimum and maximum values were -12.4 nT and 10.8 nT, respectively, with a median value of -3.2 nT. This general behavior is consistent with reports by *Murphree et al.,* [1990], who observed all their large-scale dayside features during negative B_x and positive B_y. However, here we also report the observations on April 28 (Section 3.1), when B_x was consistently positive. Figure 16

4.3. Dependence of emission on solar wind dynamic pressure

Figure 17 summarizes the dependence of the FUV emission on the solar wind Figure 17

dynamic pressure. All observations were made during periods of low dynamic pressure of less than 3 nPa. For the proton aurora observations in the cusp however, pressures as high as 38 nPa were observed and a significant positive correlation of 0.66 was found [*Frey et al.,* 2002]. Here, there is rather an indication of a negative trend, though the correlation coefficient of -0.18 is not statistically significant. The reason for this insignificance is the fact that the spot-like emission occurred intermittently during periods of constant pressure, showing impulsive increases/decreases as in the instance described in Section 3.2.

5. Discussion

There may be some concern, that the timing and solar wind propagation from the location of Wind at 260 R_e and 6 MLT may introduce uncertainties for the correlation of the spot-like emission and solar wind properties [*Collier et al.,* 1998]. The magnetosphere may interact with other field configuration than those measured at the dawn flank. However, during long time periods of this study, the solar wind properties were relatively stable and the exact timing is not crucial for most of our conclusions. There may be additional concern, that two data sets, taken two minutes apart (spin period of IMAGE) are not statistically independent. We tested this assumption by summarizing 5 consecutive data points with their minima, mean, or maxima. All major results were nevertheless very similar and we therefore presented all data points in Figures 13-17.

In a statistical study of polar cap arcs and their dependence on the IMF B_z it was found that sun-aligned arcs appeared on average with a delay of about one hour relative to a northward turning of the IMF [*Troshichev et al.,* 1988]. In this study we also found many cases when the appearance of the high latitude auroral emission was delayed with respect to changes in IMF or solar wind density/pressure. The dependence of our localized emission with regard to IMF B_y appears to be slightly different from

the occurrence of polar cap arcs. While polar cap arcs appear in the dawn sector for negative B_y and in the dusk sector for positive B_y [*Elphinstone et al.,* 1990], we could not find any spot during negative B_y conditions. It may be a specific feature of this data set, however a positive B_y may be required for the localized emission to appear, and may thus separate it morphologically from polar cap arcs.

In the past there have been reports on auroral morphology during periods of extremely low solar wind pressure. *Parks et al.* [2000] describe the aurora during 10-12 May, 1999, when the solar wind ion density dropped to values well below 1 cm^{-3} for many hours. The IMF conditions were similar to most of our cases with negative B_x, strong positive B_y and small but mostly positive B_z. At several places they mention bright "spots" of aurora, for instance at 1400 MLT, covering 78-85° of latitude. However, they concentrate on the 22 MLT region and the polar cap and energetic, uniform precipitation into it, and they do not go into much detail about the cause of the bright, localized, high latitude emission.

Hoffman et al., [1988] showed that during long periods of quiet geomagnetic conditions, the large scale region 1 and 2 currents are mostly absent, especially in mid-winter. However, small-scale field-aligned current structures were found, mostly in the cusp and polar cap, with the highest probability in summer month. Our observations here happened during April-June, a time around northern hemisphere summer.

The large time delay between the drop of solar wind densities, and the absence of obvious IMF changes related to the appearance or disappearance of the localized emission contradict a possible interpretation, that the auroral spot may be caused by the expansion of the magnetosphere under reduced external stress. Such magnetospheric expansions should occur with Alfvèn speed and new equilibrium should be reached after tens of minutes. Here we demonstrated several examples, where there were several hours of time delay between solar wind changes, and strong changes in the high latitude aurora.

In a report on the dependence of ionospheric convection and cusp field-aligned currents on the IMF B_y component, *Le et al.* [2002] describe in detail a long interval of northward IMF with strong positive B_y and negative B_x components, which happened in the later half of a magnetic cloud event on May 15, 1997. The IMF conditions were therefore very similar to most of our cases. After longer periods with high solar wind ion densities, the densities were rather low (below 4 cm^{-3}) during their key times, and therefore comparable to our situation. A combination of model calculations and measured ionospheric convection revealed that high latitude reconnection was the driver of ionospheric convection. The large positive B_y component rotated the usually sun-aligned pattern with two convection cells in the morning and afternoon regions by almost 90°. A clockwise convection cell formed on the dayside, circulating within the polar cap on open fieldlines. The second cell with counterclockwise convection formed at the nightside circulating across the polar cap boundary. This convection pattern then drives a current circuit with downward field-aligned current in the cusp region, Pedersen current in the ionosphere, and the upward field-aligned current in the polar cap in the center of the dayside convection cell.

We performed a similar model calculation of ionospheric convection with the AMIE technique [*Richmond and Kamide,* 1998]. As initialization for the model we used ground magnetometer measurements to calculate the ionospheric convection (not shown here) and the field-aligned currents. Figure 18 shows the result at 18:36 UT during the WIC observations and simultaneous FAST measurements (Figures 9-12) which is representative for several other model runs during other time periods. The calculations show and FAST measurements confirm that a downward field-aligned current exists on the dayside with cusp particle signatures (76-81° latitude, 9-16 MLT). At higher latitudes (80-90^c*irc* latitude and 14-18 MLT), where the localized strong electron aurora is concentrated, upward field-aligned currents are found. The mapping of this region confirmed, that it is not connected to the high latitude magnetosphere, where

Figure 18

reconnection may occur. Instead, it is magnetically connected to regions far in the tail. Therefore, the strong electron aurora can not be the direct result of reconnection under northward IMF. These observations support in large parts the results of *Le et al.,* [2002]. What we add here is the temporal behavior of the aurora, which in several cases shows significant, rapid changes in brightness.

We deliberately did not include FAST and FUV measurements as input into the AMIE model runs, because we did not want to force the results into a specific direction but rather preferred using ground magnetometer measurements only. The results are very encouraging as they show a very good agreement with the location of major regions from FAST and FUV measurements. Incorporation of flux and mean energy of precipitating electrons from FUV measurements as parameters for the ionospheric conductivity did actually not much change the results (not shown here).

It is clear that the localized strong electron aurora appears at the footpoint of the upward field-aligned current leg of the large-scale current circuit, which in turn may be driven by high latitude reconnection. All our observations were performed during periods of very low solar wind dynamic pressure and northward IMF, which should have allowed the magnetosphere to expand to a greater than usual size. This expansion should have reduced the plasma density in the magnetosphere and magnetosheath. However, the continued northward IMF drives reconnection in the anti-parallel merging region, which drives the current circuit. At some point the source region of the upward field-aligned current should be depleted and unable to further provide enough current for the circuit. At this point a field-aligned potential builds up, which accelerates electrons in order to continue the current flow. Protons from the source region can not overcome this potential whenever their energy is not high enough and that explains the complete lack of ions in the FAST spectra. This field-aligned potential furthermore explains the inverted-V like structures in the FAST electron spectra.

In an investigation of X-ray images and coincident DMSP satellite particle

measurements during a period of low solar wind density *Anderson et al.,* [2000] found an intense emission and multi-component precipitation at high latitude. They interpreted the lower-energy component (few hundred eV) as suprathermal electrons from the solar wind, and the higher-energy component (centered around 7 keV) as electrons which were accelerated in solar flares. The solar wind conditions were very similar to most of our cases with low density, negative B_x and positive B_y and B_z. During several of our coincident FAST passes, we observe similar two electron components in the polar cap with energies below 100 eV and around 400-1000 eV in the polar cap (not shown here). Here, we concentrate on the very localized emission which they describe as "inverted-V' electron fluxes at the dusk side above 80° latitude (see Figure 1 in [*Anderson et al.,* 2000], and which they claim would have produced little in the way of X-ray fluxes to be observed by PIXIE because their energies were too low. These electrons should have produces intense FUV emission. Furthermore, our mapping results show, that these regions map into the magnetotail, rather than to field lines with direct connection to the solar wind.

6. Conclusions

We performed a statistical investigation of the properties of localized, bright FUV emission at the dayside high latitudes, which are frequently observed by the FUV instrument on IMAGE. The much higher latitude location, the requirement for low solar wind densities and positive IMF B_y, and the complete absence of proton precipitation separate this phenomenon from the previously described proton aurora in the cusp [*Frey et al.,* 2002]. The only similarity between both phenomena is the occurrence during northward IMF conditions.

While the proton aurora in the cusp is the result of direct precipitation after high latitude reconnection, we think that the electron aurora here has a different cause. Coincident particle measurements by FAST confirm, that there is still proton

precipitation along the downward field-aligned current into the cusp at lower latitude (see Figures 8 and 11). However, the energy and flux of these protons are too low to create a significant signal in the SI-12 imager. They further confirm that upward currents at higher latitudes with electrons of inverted-V spectra create the bright FUV emission seen in WIC.

The mapping of field lines shows that the downward current region maps close to the magnetopause, where these fieldlines may reconnect with the draped field in the magnetosheath allowing for direct precipitation into the cusp. Fieldlines from the electron aurora spots map into the distant magnetotail and are unlikely to merge with the solar wind.

Model calculations with the AMIE technique confirm, that during the period with large positive IMF B_y and northward IMF, the general two-cell convection pattern in the ionosphere is very much distorted. The locations of the upward and downward field-aligned currents coincide with the location of FUV observations. The spectral shape of electrons precipitating into the localized FUV emission indicates the existence of a field-aligned potential drop, which accelerates electrons into inverted-V spectra and most likely reflects protons and inhibits precipitation. The driver for the convection is reconnection at high latitudes which in turn creates the downward and return currents [*Le et al.,* 2002]. What we add here to this previous observation is the analysis of the major properties of the aurora and the observation of temporal changes. These fluctuations in the auroral brightness might be interpreted as the result of pulsed reconnection and therefore pulsed upward currents. However, the time scales of these fluctuations are too long (30-70 minutes) for pulsed reconnection. We rather think that these fluctuations represent temporal changes in the upward field-aligned potential probably caused by drops in local density due to evacuation.

Acknowledgments. We are grateful to the IMAGE-SMOC team who keep the IMAGE

spacecraft running. The IMAGE FUV investigation was supported by NASA through SwRI subcontract number 83820 at the University of California at Berkeley under contract number NAS5-96020. The solar wind measurements were obtained from CDAWeb. We acknowledge the following PIs: Wind Magnetic Fields Investigation: R. Lepping; Wind Solar Wind Experiment: K. Ogilvie; Geotail Magnetic Field Instrument: S. Kokubun; Geotail Comprehensive Plasma Instrument: L. Frank.

References

Andersen, P. C., D. L. McKenzie, D. W. Datlowe, J. D. Hawley, S. M. Petrinec, M. Schulz, and D. E. Larson, Polar cap X-rays and electrons under low density solar wind conditions: Coordinated PIXIE and DMSP observations on 11 May 1999, *Geophys. Res. Lett., 27,* 4021, 2000.

Collier, M. R., J. A. Slavin, R. P. Lepping, A. Szabo, and K. Ogilvie, Timing accuracy for the simple planar propagation magnetic field structures in the solar wind, *Geophys. Res. Lett., 25,* 2509, 1998.

Drury, E. E., S. B. Mende, H. U. Frey, J. H. Doolittle, Southern hemisphere poleward moving auroral forms, submitted to *J. Geophys. Res.,* 2002.

Elphinstone, R. D., K. Jankowska, J. S. Murphree, and L. L. Cogger, The configuration of the auroral distribution for interplanetary magnetic field B_z northward, 1. IMF B_x and B_y dependence as observed by the Viking satellite, *J. Geophys. Res., 95,* 5791, 1990.

Elphinstone, R. D., D. J. Hearn, J. S. Murphree, L. L. Cogger, M. L. Johnson, and H. B. Vo, Some UV dayside auroral morphologies, in *Auroral Plasma Dynamics,* AGU Geophysical Monograph 80, AGU, Washington, 1993.

Fasel, G. J. Dayside poleward moving auroral forms: A statistical study, *J. Geophys. Res., 100,* 11891, 1995.

Frey, H. U., S. B. Mende, C. W. Carlson, J.-C. Geŕard, B. Hubert, J. Spann, R. Gladstone, and T. J. Immel, The electron and proton aurora as seen by IMAGE-FUV and FAST, *Geophys. Res. Lett., 28,* 1135, 2001.

Fuselier, S. A., H. U. Frey, K. J. Trattner, S. B. Mende, and J. L. Burch, Cusp aurora dependence on IMF B_z, accepted by *J. Geophys. Res.,* 2002.

Gladstone, G. R. et al., Stellar calibration of the WIC and SI imagers and the GEO photometers on IMAGE/FUV, *Poster presented at AGU Fall Meeting,* 2000.

Hoffman, R. A., M. Sugiura, N. C. Maynard, R. M. Candey, J. D. Craven, and L. A. frank, Electrodynamic patterns in the polar region during periods of extreme magnetic quiescene, *J. Geophys. Res., 93,* 14515, 1988.

Le, G., G. Lu, R. J. Strangeway, and R. F. Pfaff, Strong IMF B_y-related plasma convection in the ionosphere and cusp field-aligned currents under northward IMF conditions, submitted to *J. Geophys. Res.*, 2002.

Mende, S. B. et al., Far ultraviolet imaging from the IMAGE spacecraft, *Space Sci. Rev., 91,* 287, 2000.

Milan, S. E., M. Lester, S. W. H. Cowley, and M. Brittnacher, Dayside convection and auroral morphology during an interval of northward interplanetary magnetic field, *Ann. Geophys., 18,* 436-444, 2000.

Murphree, J. S. and R. D. Elphinstone, Correlative studies using the Viking imagery, *Adv. Space Res., 8,* 9, 1988.

Murphree, J. S., R. D. Elphinstone, D. Hearn, and L. L. Cogger, Large-scale high-latitude dayside auroral emissions, *J. Geophys. Res., 95,* 2345, 1990.

Ohtani, S., R. D. Elphinstone, O. A. Troshichev, M. Yamauchi, L. Blomberg, L. J. Zanetti, and T. A. Potemra, Response of the dayside auroral and electrodynamic processes to variations in the interplanetary magnetic field, *J. Geophys. res., 102,* 22247, 1997.

Parks, G., M. Brittnacher, D. Chua, M. Fillingim, G. Germany, and J. Spann, Behavior of the aurora during 10-12 May, 1999 when the solar wind nearly disappeared, *Geophys. Res. Lett., 27,* 4033, 2000.

Richmond, A.D., and Y. Kamide, Mapping electrodynamic features of the high-latitude ionosphere from localized observations: Technique, *J. Geophys. Res., 93,* 5741, 1988.

Sandholt, P. E., C. J. Farrugia, J. Moen, O. Noraberg, B. Lybekk, T. Sten, and T. Hansen, A classification of dayside auroral forms and activities as a function of interplanetary magnetic field orientation, *J. Geophys. Res., 103,* 23325, 1998.

Sandholt, P. E. and C. J. Farrugia, On the dynamic cusp aurora and IMF B_y, *J. Geophys. Res., 104,* 12461, 1999.

Smith, M. F. and M. Lockwood, Earth's magnetospheric cusps, *Rev. Geophys., 34,* 233, 1996.

Troshichev, O. A., M. G. Gusev, S. V. Nickolashkin, and V. P. Samsonov, Features of the polar cap aurorae in the southern polar region, *Planet. Space Sci/, 36,* 429, 1988

Tsyganenko, N. A., Modeling the Earth's magnetospheric magnetic field confined within a

realistic magnetopause, *J. Geophys. Res., 100,* 5599, 1995.

Tsyganenko, N. A. and D. P. Stern, A new-generation global magnetosphere field model, based on spacecraft magnetometer data, *ISTP Newsletter, 6,* 21, 1996.

Walker, I. K., J. Moen, L. Kersley, and D. A. Lorentzen, On the possible role of cusp/cleft precipitation in the formation of polar-cap patches, *Ann. Geophys., 17,* 1298-1305, 1999.

Zhu, L., R. W. Schunk, and J. J. Sojka, Polar cap arcs: a review, *J. Atmos. Solar-Terr. Phys., 59,* 1087, 1997.

H. U. Frey, J. Bonnell, T. J. Immel, N. Østgaard, Space Sciences Laboratory, University of California, Berkeley, CA 94720-7450 (e-mail: hfrey@ssl.berkeley.edu)

B. Hubert, LPAP, Université de Liège,B-4000 Liège, Belgium (e-mail: benoit@astro.ulg.ac.be)

G. Le, Laboratory for Extraterrestrial Physics, Code 696, NASA Goddard Space Flight Center, Greenbelt, MD 20771, USA (email: Guan.Le@gsfc.nasa.gov)

G. Lu, High Altitude Observatory, NCAR, 3450 Mitchell Lane,Boulder, CO 80301, USA (e-mail: ganglu@hao.ucar.edu)

S.A. Fuselier, Lockheed Martin ATC, 3251 Hanover St., Palo Alto, CA 94304-1191 (e-mail: stephen.a.fuselier@lmco.com)

Received ??? 2002; revised ??? 2002; accepted ??? 2002.

---

[1]Space Sciences Laboratory, University of California, Berkeley, USA

[2]High Altitude Observatory, National Center for Atmospheric Research, Boulder, USA

[3]Lockheed Martin ATC, Palo Alto, USA

[4]LPAP, Université de Liège, Liège, Belgium

[5]NASA, Goddard Space Flight Center, Greenbelt, USA

To appear in the *Journal of Geophysical Research*, 2002.

Figure 1. Examples of observations of WIC (top row) and the corresponding proton images (bottom row) for four different days in 2001. The original images were re-mapped into a MLT-latitude grid with local noon at the top, midnight at the bottom, and dawn to the right of each image.

Figure 2. Observation of WIC (top row), SI-13 (middle row), and SI-12 (lowest row) on April 28, 2001 at 21:06:18 (left) and 21:22:39 (right).

Figure 3. Summary of ultraviolet observations and related, propagated solar wind parameters for April 28, 2001 (doy=118). The panels from top to bottom show the time shifted solar wind proton density (Wind solid line, Geotail dashed line), the Wind-measured IMF-GSM B_z (solid line), B_y (dashed line), and B_x (dotted line) components, the proton aurora emission (instrument counts), the brightest emission in the wide-band imaging camera (instrument counts) and the oxygen imager (instrument counts) in the corresponding regions.

Figure 4. Examples of observations by the WIC imager on May 25, 2001. The format is the same as in Figure 1.

Figure 5. Summary of ultraviolet observations and related solar wind parameters for May 25, 2001. The format is similar to Figure 3 with the two last panels showing the geomagnetic latitude and MLT of the brightest emission in the WIC images.

Figure 6. Summary of solar wind and FUV observations on May 25/26.

Figure 7. Mapped WIC image taken on May 26, 2001 at 01:17:13 with the footpoint along the FAST satellite track from one minute before to 3 minutes after image integration. The footpoint of FAST at image integration is given by the small asterisk.

Figure 8. Summary of FAST measurements and FUV observations on May 26, 2001. The top panel shows the magnetic field disturbances with the green line representing the cross-track component. The next panel is the ion energy spectrogram in the loss cone. Then follow the electron energy spectrogram averaged over all pitch angles, and the pitch angle distribution. The next two panels summarize the energy fluxes of electrons and ions, mapped to 100 km altitude. The last two panels are the count rates in the six consecutive WIC and SI-12 images along the footpoint of FAST.

Figure 9. Summary of solar wind and FUV observations on May 24.

Figure 10. WIC image and track of the FAST satellite through the 18:46:39 UT image on May 24. The line represents the track from one minute before to three minutes after the image exposure.

Figure 11. Summary of FAST measurements and FUV observations on May 24, 2001. The format is the same as in Figure 8.

Figure 12. Result of field line mapping from the auroral region into the magnetosphere. The bottom middle panel shows the original WIC image taken at 18:46:39 on May 24, 2001. Six points around the perimeter of the localized strong emission were mapped into the magnetosphere together with two field lines originating in the dark region of downward current, as determined by the FAST measurements in Figure 11. The three top panels show these field lines looking from dusk, from the sun, and from above the north pole, respectively. The bottom left panel shows these field lines in the rotated plane.

Figure 13. Distribution of observations in magnetic local time and geomagnetic latitude. The mean and median values are similar with 82.4° latitude and 14.6 hours magnetic local time.

Figure 14. Dependence of the latitude location and broadband FUV brightness on the value of the IMF B_z.

Figure 15. Dependence of the local time location and broadband FUV brightness on the value of IMF B_y. The top panel also shows the least square fitted linear relation of MLT=13.2 + 0.205B_y.

Figure 16. Dependence of the local time location on the value of IMF B_x.

Figure 17. Dependence of the latitude location and broadband FUV brightness on the solar wind dynamic pressure. The lower panel also shows the least square fitted linear relation of WIC = 1100 - 206 p_{dyn}.

Figure 18. AMIE model calculations of field-aligned currents for the time of the FAST pass through the bright localized emission and the mapping in Figure 12. Solid contours indicate downward current, dashed contours show upward currents.

Table 1. Summary of all events used for this study. The time intervals are given in UT of FUV observations. The solar wind values are shifted for the propagation time. Density values show the range and mean in cm^{-3}. The magnetic field values show the range and mean values in nT, rounded to the nearest integer.

Date and Time	Density	B_x	B_y	B_z
2001-114, 13:35-17:59	2.8-4.6 (3.4)	-5 to +2 (-3)	+3 to +10 (+7)	-1 to +7 (+4)
2001-118, 21:00-21:33	0.9-1.9 (1.4)	+5 to +6 (+5)	+8 to +10 (+9)	+2 to +7 (+5)
2001-119, 03:00-07:46	1.9-4.0 (2.9)	-8 to -4 (-7)	+5 to +9 (+7)	+0 to +5 (+2)
2001-119, 17:15-17:59	0.6-2.5 (1.6)	-3 to -2 (-3)	+1 to +3 (+2)	+3 to +4 (+4)
2001-144, 03:17-09:25	1.2-5.8 (1.7)	-8 to -1 (-5)	+5 to +10 (+8)	-4 to +4 (+2)
2001-144, 13:52-23:33	0.6-2.7 (1.1)	-7 to +1 (-4)	+1 to +8 (+6)	-1 to +5 (+2)
2001-145, 03:33-14:25	0.9-2.0 (1.3)	-7 to +1 (-4)	-1 to +7 (+5)	-5 to +5 (+1)
2001-145, 18:52-03:20	1.4-3.7 (2.1)	-3 to +6 (+2)	-1 to +6 (+3)	-3 to +4 (+2)
2001-146, 08:48-15:55	0.8-3.1 (1.6)	-4 to +2 (-3)	-1 to +5 (+3)	-3 to +4 (+3)
2001-147, 15:26-22:13	1.4-4.6 (2.9)	-7 to +11 (+1)	-4 to +13 (+9)	-4 to +12 (+6)
2001-148, 03:25-05:40	2.7-4.3 (3.4)	-3 to +3 (+0)	+3 to +8 (+7)	-6 to +6 (+2)
2001-149, 07:04-10:43	1.6-5.1 (2.9)	+2 to +4 (+3)	+6 to +8 (+7)	+0 to +7 (+4)
2001-170, 02:21-11:21	0.7-3.2 (1.4)	-12 to +0 (-7)	+9 to +16 (+12)	+0 to +9 (+3)

Figure 1

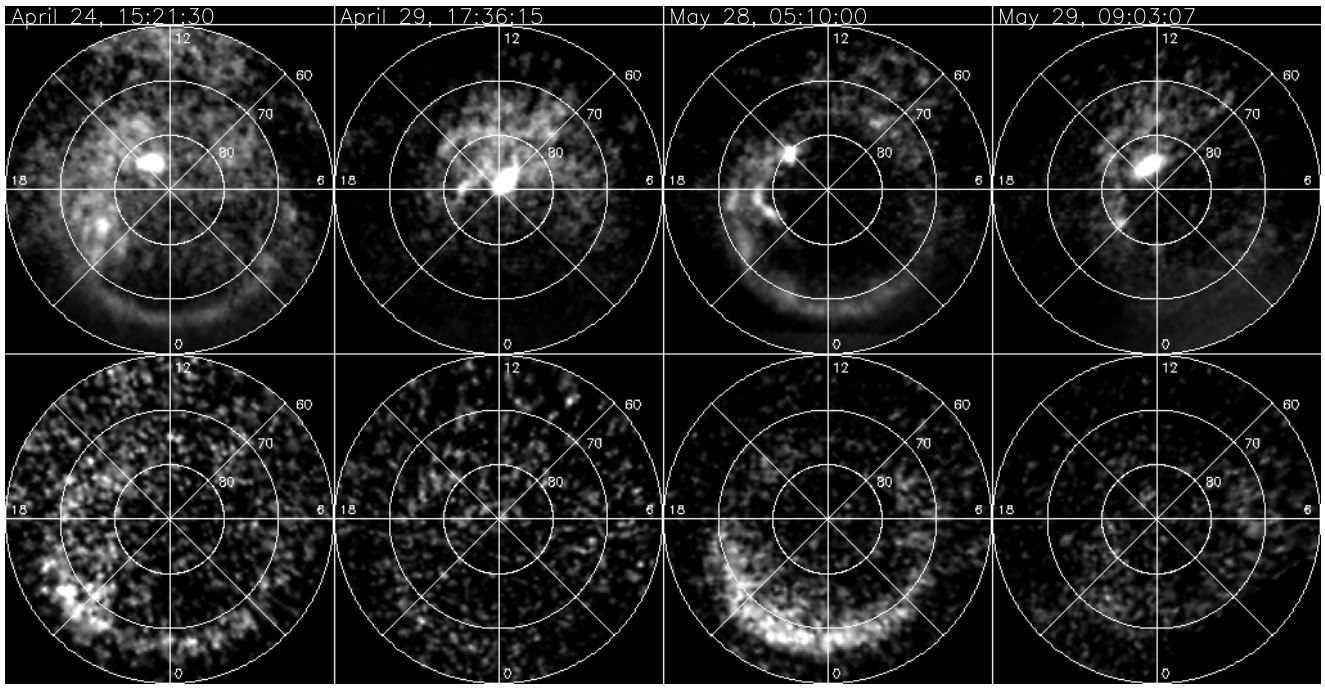

Wed Jan 9 12:44:31 2002, hfrey
/disks/sprite/disk1/hfrey/idl/image/lowdens/show_low_examples

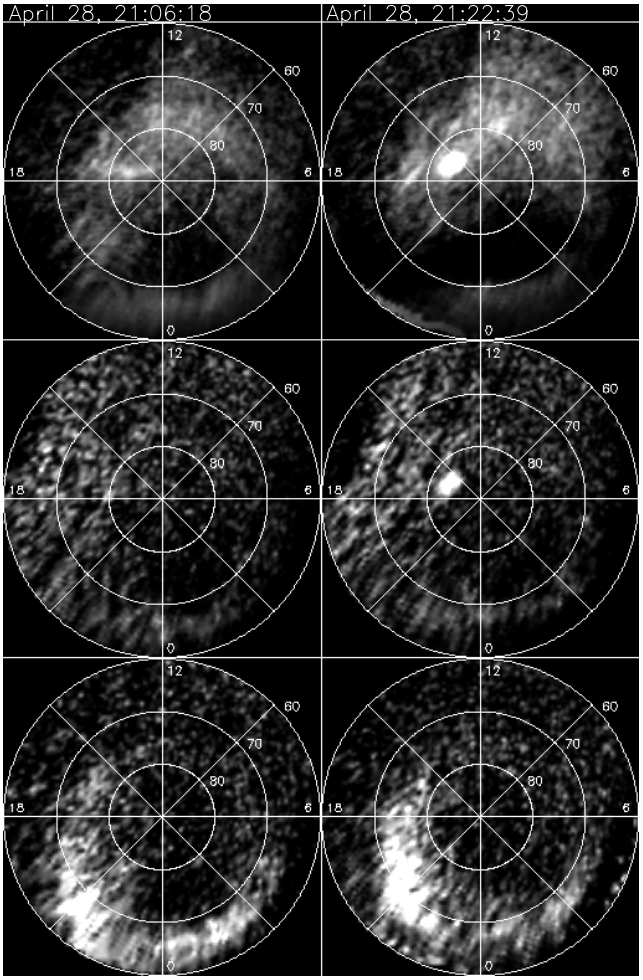
April 28, 21:06:18
April 28, 21:22:39
12
60
70
80
18
6
0
Wed Jan 9 13:21:43 2002, hfrey
/disks/sprite/disk1/hfrey/idl/image/lowdens/figures_118

Figure 2

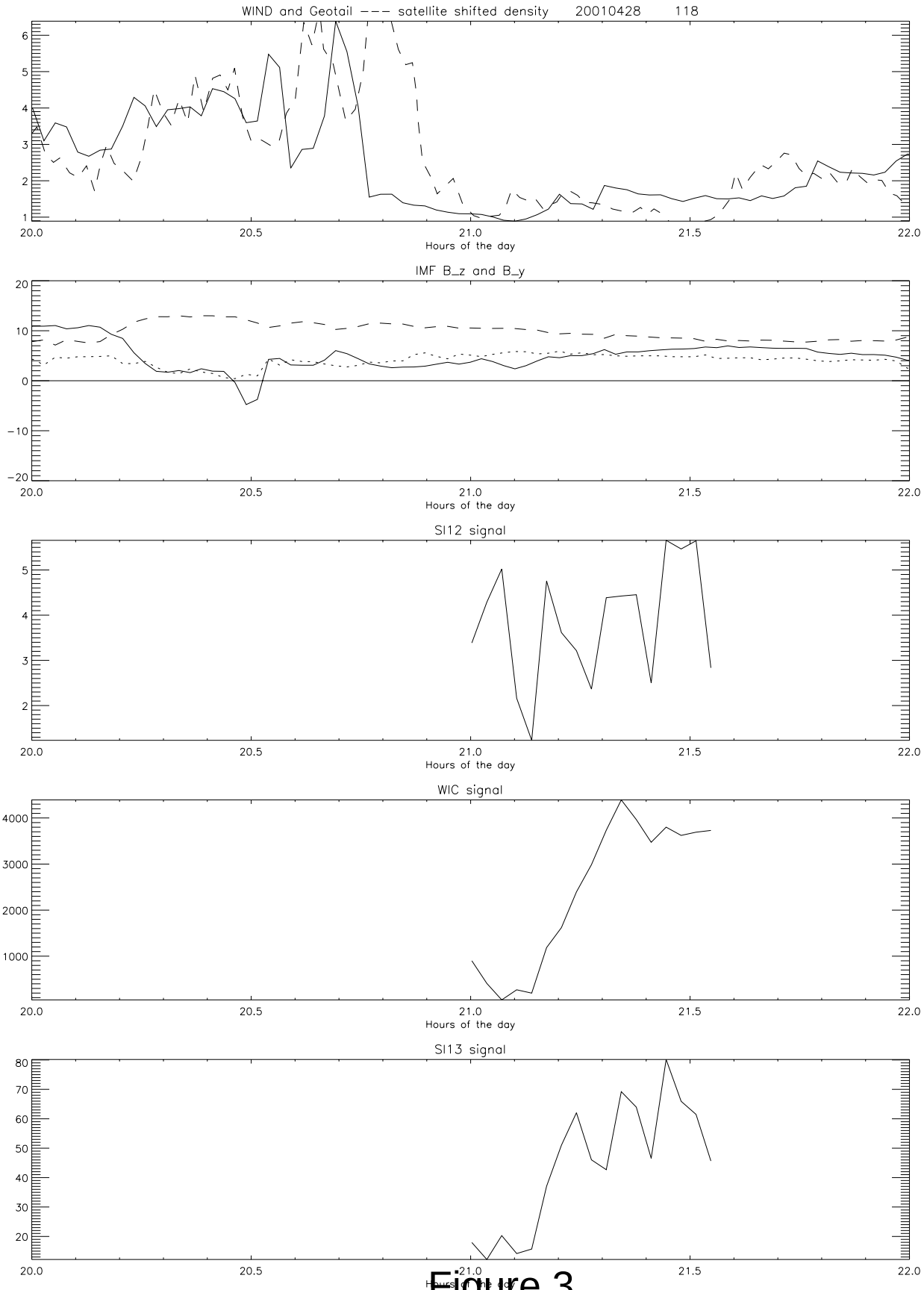
WIND and Geotail --- satellite shifted density 20010428 118
Hours of the day
IMF B_z and B_y
Hours of the day
SI12 signal
Hours of the day
WIC signal
Hours of the day
SI13 signal
Hours of the day
Thu Jan 10 13:54:23 2002, hfrey
/disks/sprite/disk1/hfrey/idl/image/lowdens/plot_ace_wind_geo_data_full

Figure 3

Figure 4

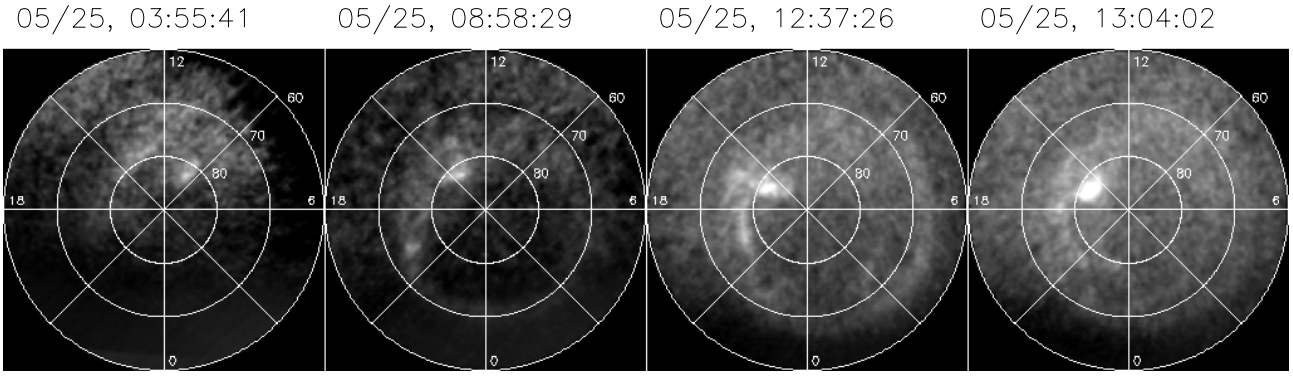

Wed Feb 13 12:55:27 2002, hfrey
/disks/sprite/disk1/hfrey/idl/image/lowdens/show_low_145

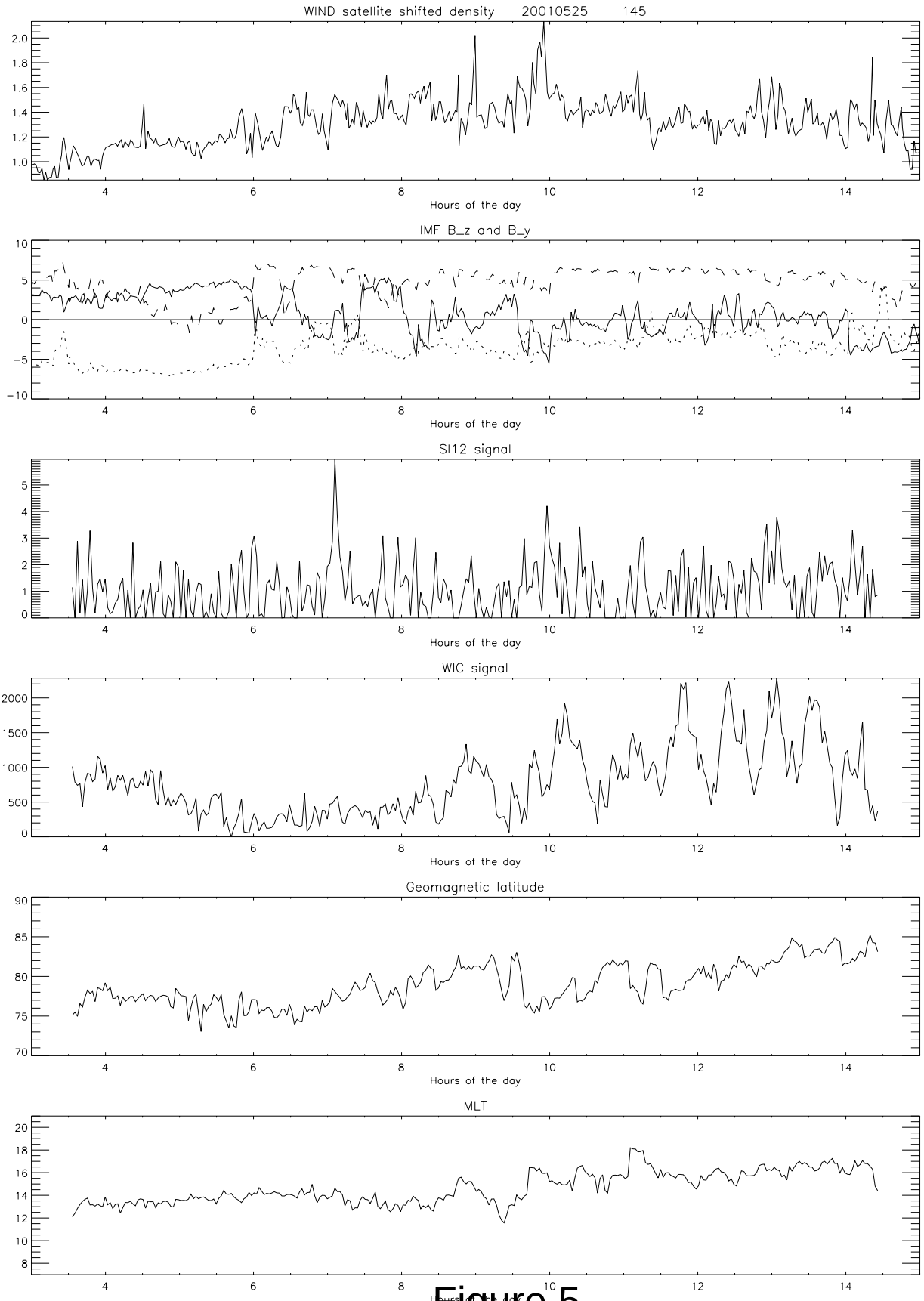

Thu Jan 10 14:05:47 2002, hfrey
/disks/sprite/disk1/hfrey/idl/image/lowdens/plot_ace_wind_geo_data_full

Figure 5

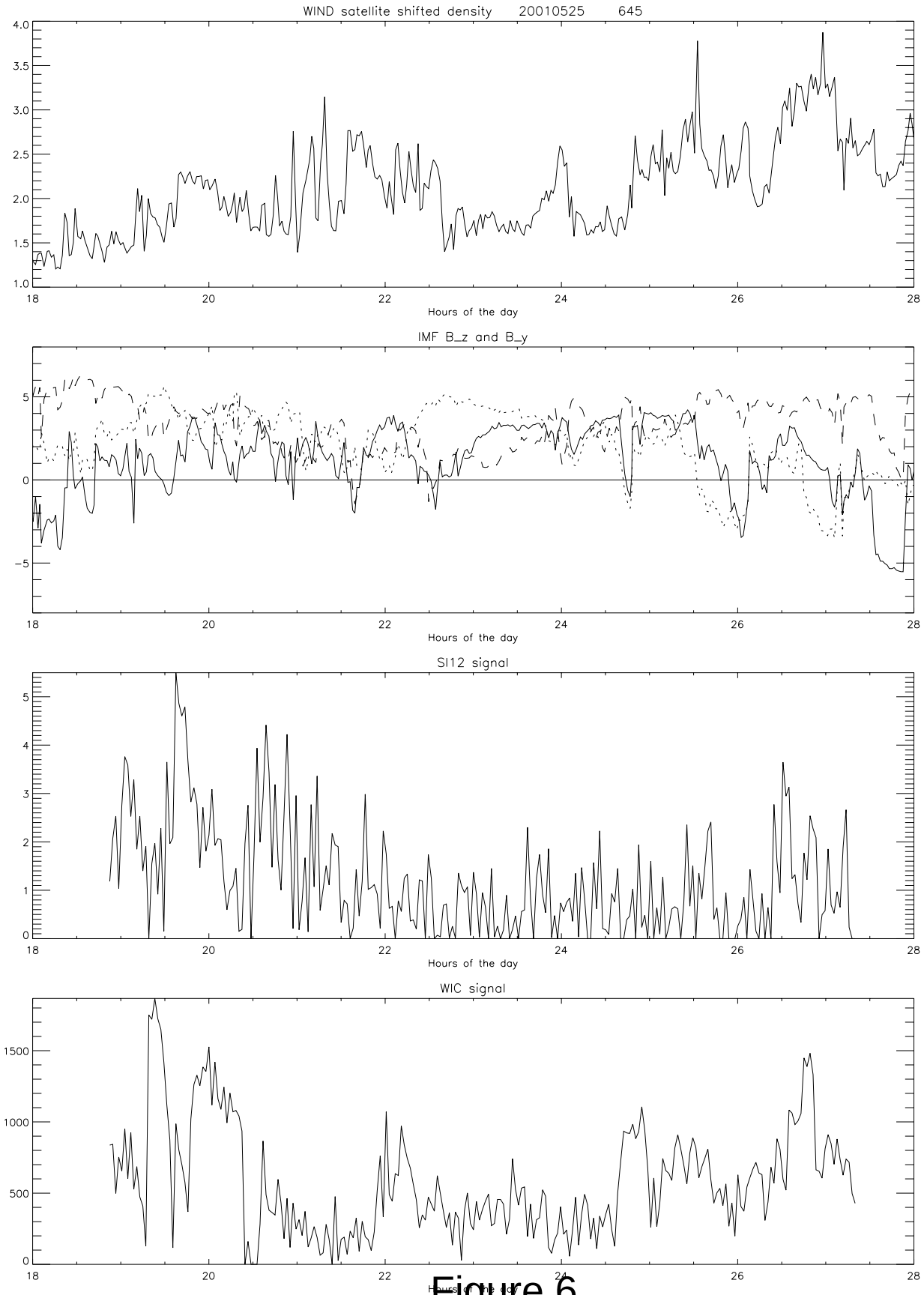

Wed Jan 16 16:17:59 2002, hfrey
/disks/sprite/disk1/hfrey/idl/image/lowdens/plot_ace_wind_geo_data_full

Figure 6

Figure 7

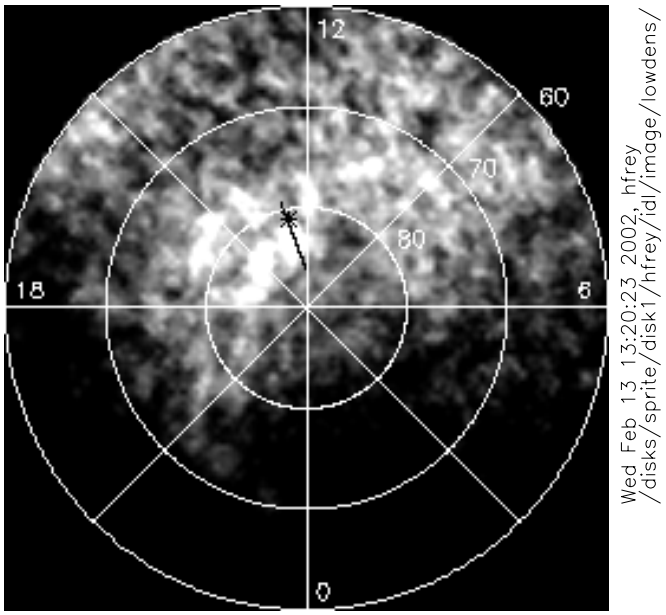
12
60
70
80
18
6
0
Wed Feb 13 13:20:23 2002, hfrey
/disks/sprite/disk1/hfrey/idl/image/lowdens/

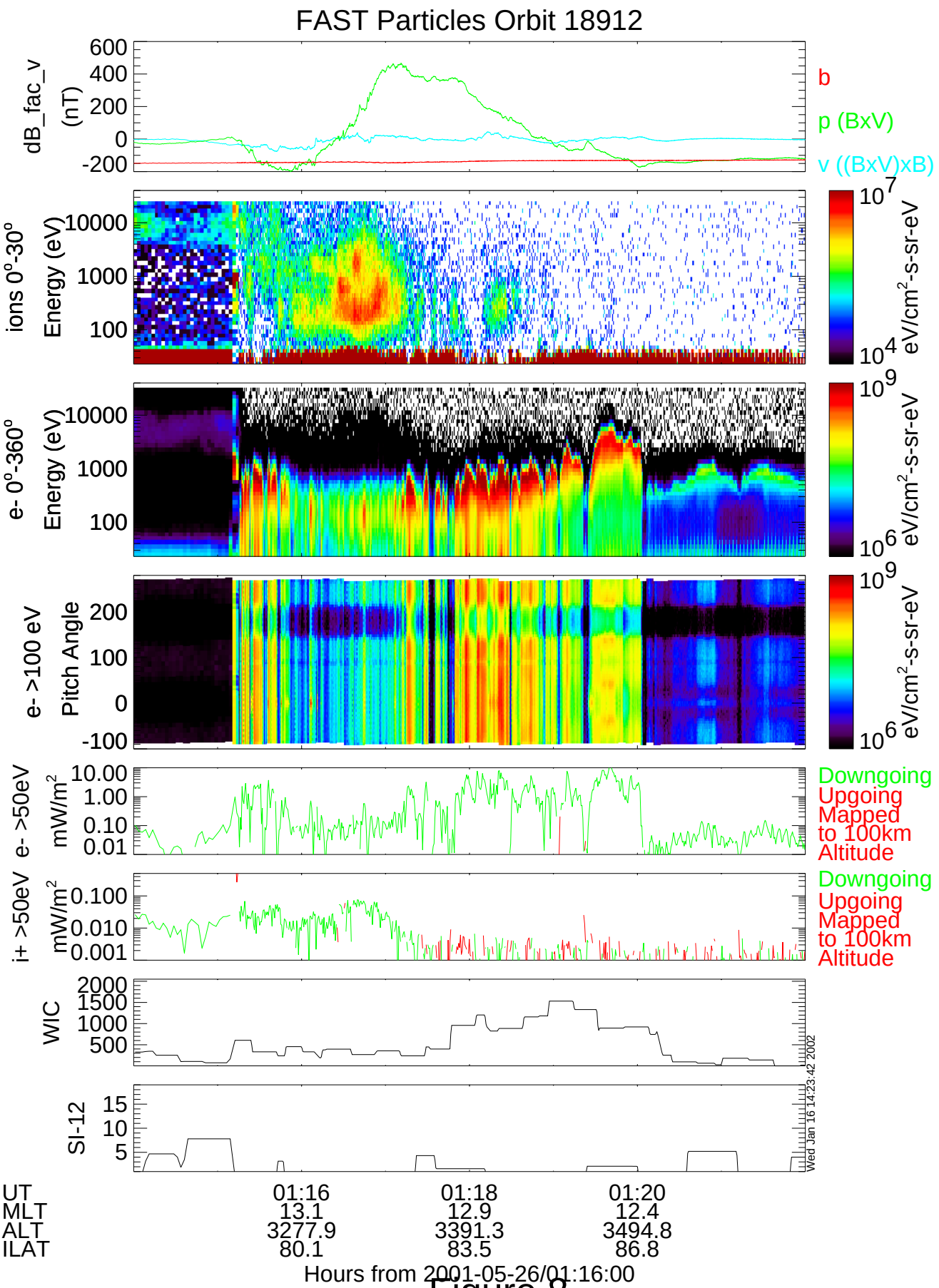
FAST Particles Orbit 18912
dB_fac_v (nT)
600
400
200
0
-200
b
p (BxV)
v ((BxV)xB)
ions 0°-30°
Energy (eV)
10000
1000
100
10^7
10^4
eV/cm^2-s-sr-eV
e- 0°-360°
Energy (eV)
10000
1000
100
10^9
10^6
eV/cm^2-s-sr-eV
e- >100 eV
Pitch Angle
200
100
0
-100
10^9
10^6
eV/cm^2-s-sr-eV
e- >50eV
mW/m^2
10.00
1.00
0.10
0.01
Downgoing
Upgoing
Mapped
to 100km
Altitude
i+ >50eV
mW/m^2
0.100
0.010
0.001
Downgoing
Upgoing
Mapped
to 100km
Altitude
WIC
2000
1500
1000
500
SI-12
15
10
5
Wed Jan 16 14:23:42 2002
UT 01:16 01:18 01:20
MLT 13.1 12.9 12.4
ALT 3277.9 3391.3 3494.8
ILAT 80.1 83.5 86.8
Hours from 2001-05-26/01:16:00

Figure 8

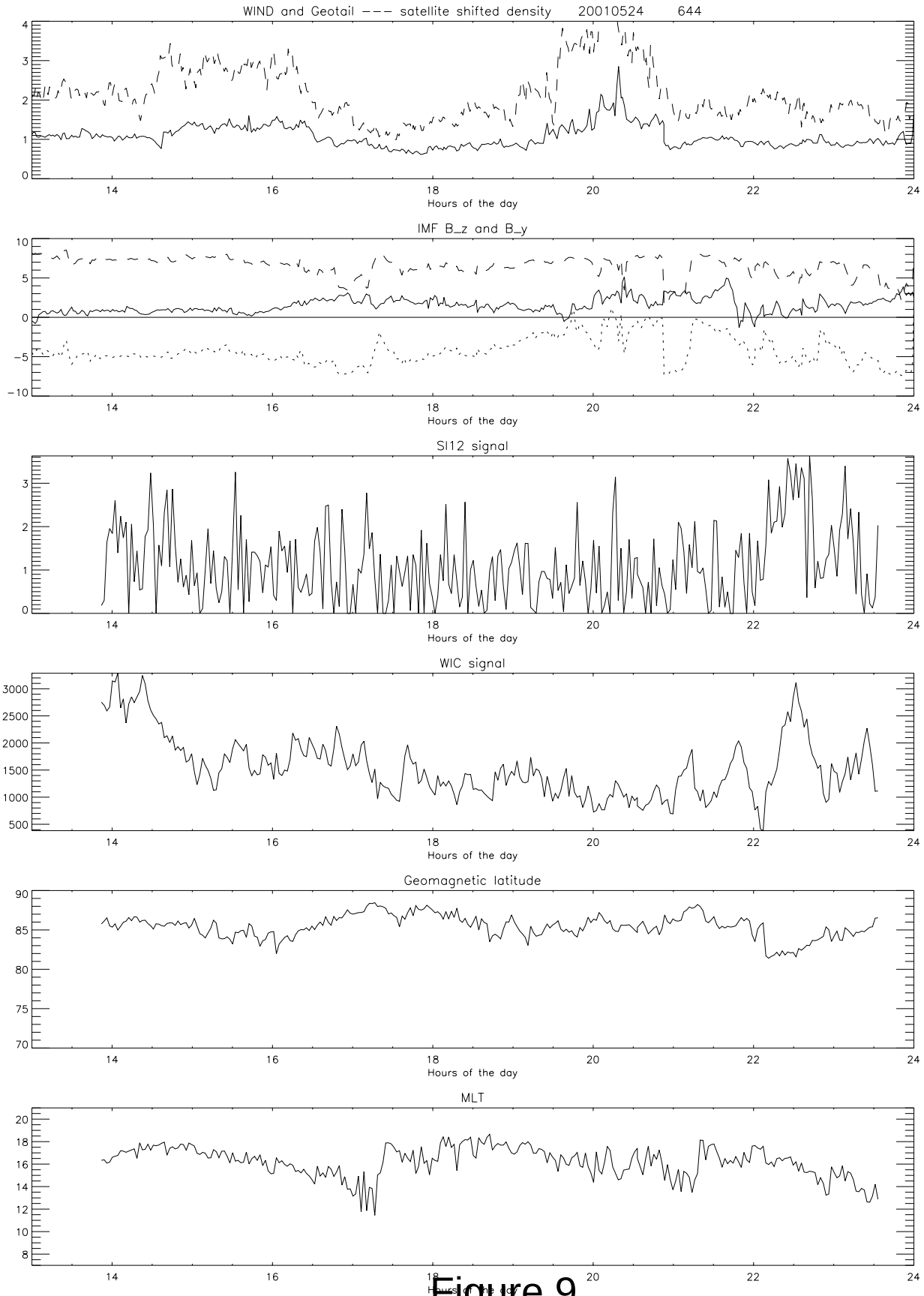

Wed Jan 16 18:33:48 2002, hfrey
/disks/sprite/disk1/hfrey/idl/image/lowdens/plot_ace_wind_geo_data_full

Figure 9

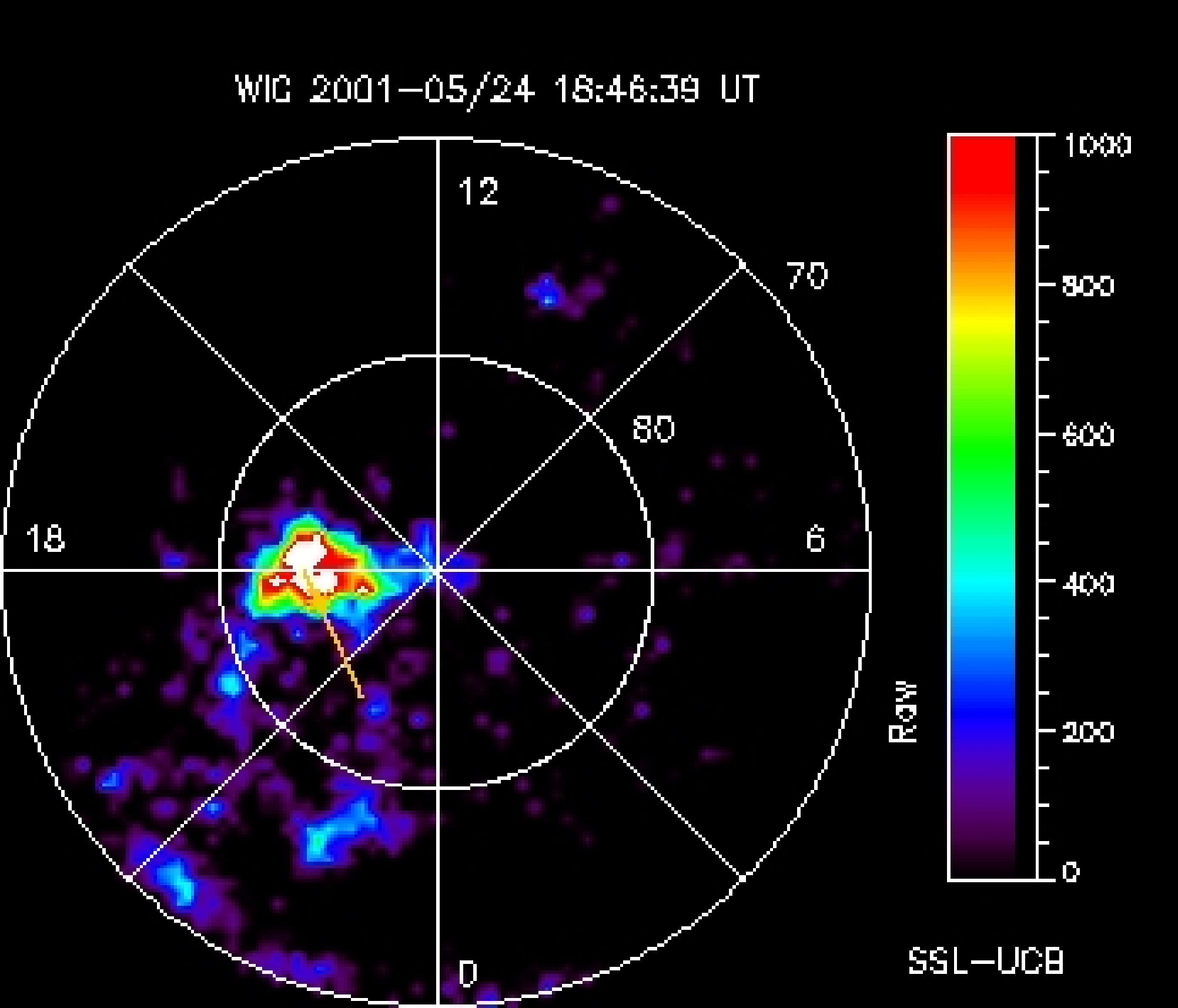
WIC 2001-05/24 18:46:39 UT
12
70
80
18
6
0
1000
800
600
400
200
0
RAW
SSL-UCB

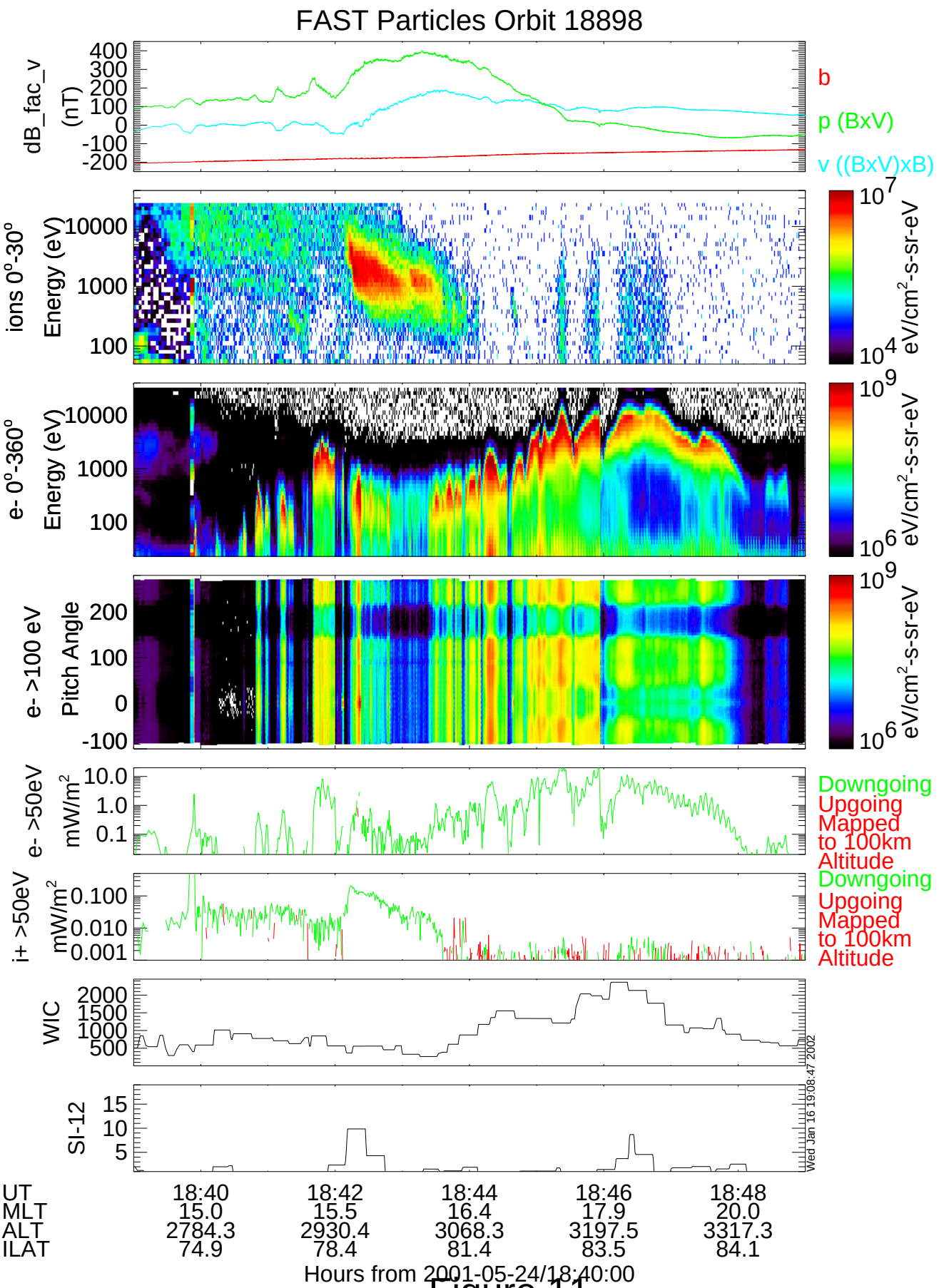
FAST Particles Orbit 18898
dB_fac_v (nT)
400
300
200
100
0
-100
-200
b
p (BxV)
v ((BxV)xB)
ions 0°-30°
Energy (eV)
10000
1000
100
10^7
10^4
eV/cm^2-s-sr-eV
e- 0°-360°
Energy (eV)
10000
1000
100
10^9
10^6
eV/cm^2-s-sr-eV
e- >100 eV
Pitch Angle
200
100
0
-100
10^9
10^6
eV/cm^2-s-sr-eV
e- >50eV
mW/m^2
10.0
1.0
0.1
Downgoing
Upgoing
Mapped
to 100km
Altitude
i+ >50eV
mW/m^2
0.100
0.010
0.001
Downgoing
Upgoing
Mapped
to 100km
Altitude
WIC
2000
1500
1000
500
SI-12
15
10
5
Wed Jan 16 19:08:47 2002
UT 18:40 18:42 18:44 18:46 18:48
MLT 15.0 15.5 16.4 17.9 20.0
ALT 2784.3 2930.4 3068.3 3197.5 3317.3
ILAT 74.9 78.4 81.4 83.5 84.1
Hours from 2001-05-24/18:40:00

Figure 11

IMAGE/WIC
24-May-2001 (01144) Time: 18 46 39
Tilt Angle: 29.7 deg
Dst: 8 nT

WIND
Time: 18 33 30.2 Delay: 12.5 min
DynP: 0.4 nPa Bswx: -3.9 nT
Bswy: 6.6 nT Bswz: 1.1 nT

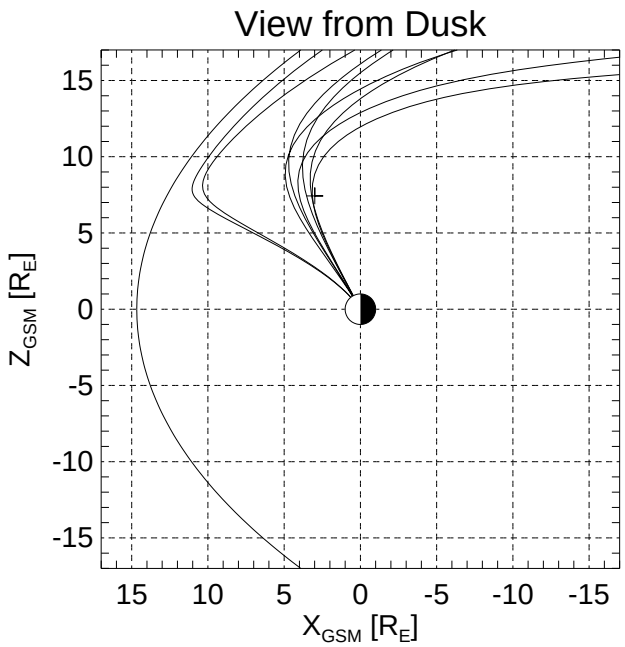

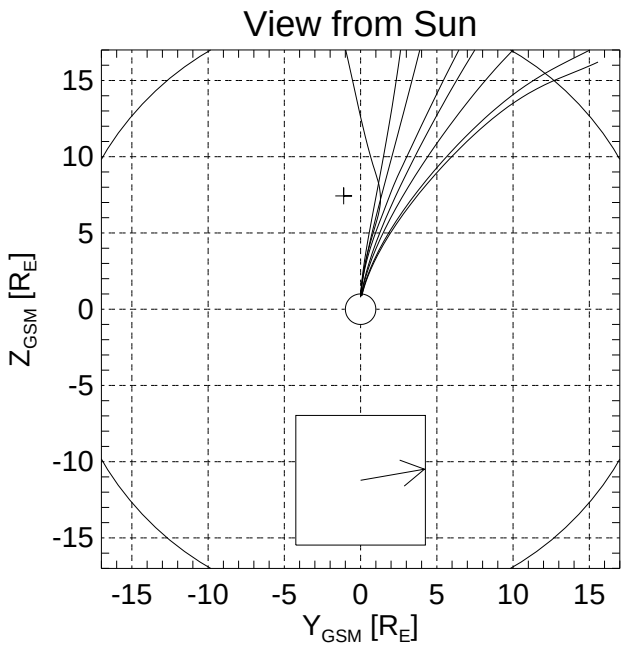

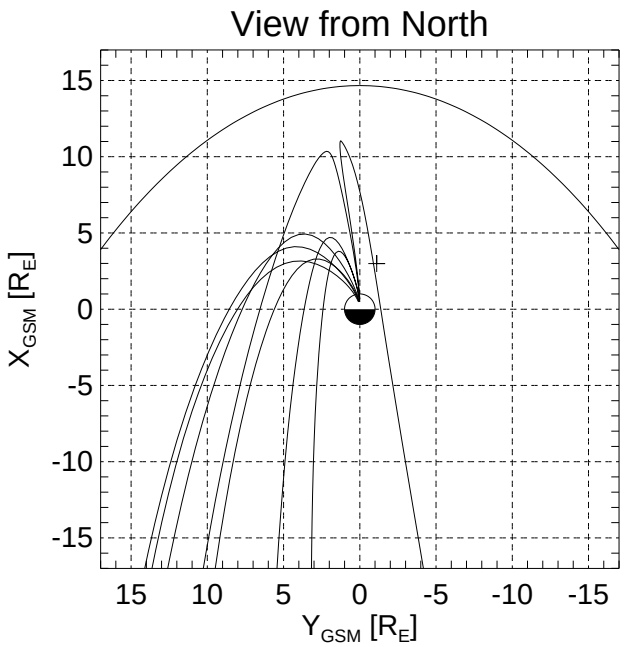

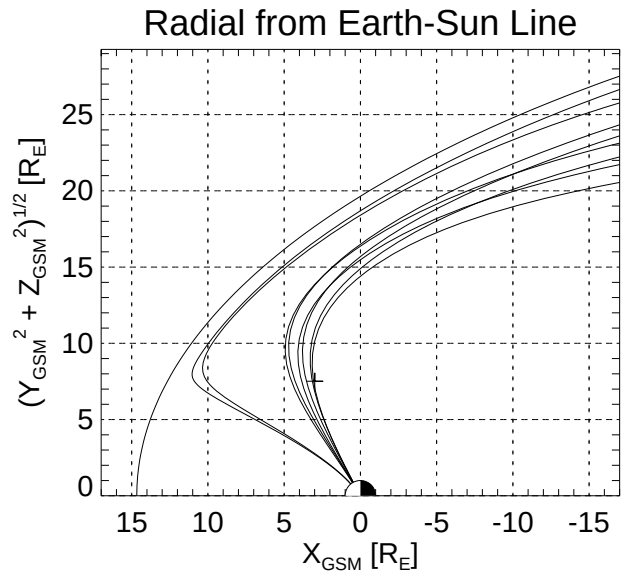

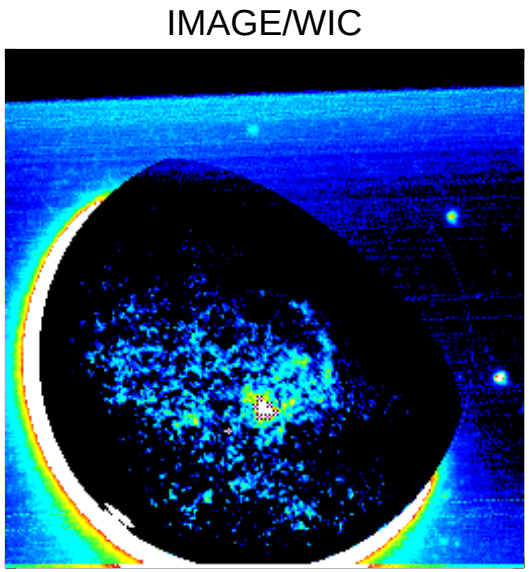

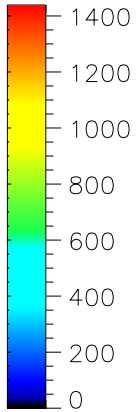

Lat, N	Lon, E	Indices
70.92	271.81	(109,67)
71.13	273.10	(110,67)
77.05	310.88	(133,76)
79.20	305.69	(130,80)
80.68	292.39	(125,83)
78.67	288.71	(123,79)
76.39	294.35	(125,74)
76.38	302.28	(129,74)

Ver. 1.6
13-Feb-2002

Figure 12

Figure 13

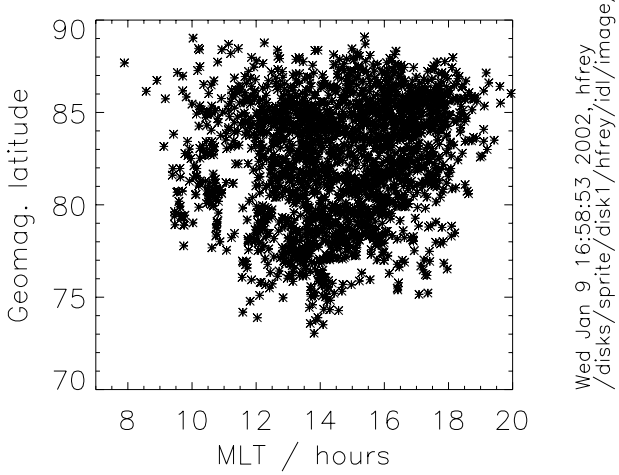

Wed Jan 9 16:58:53 2002, hfrey
/disks/sprite/disk1/hfrey/idl/image/lowdens/mach_all_lowdens_figures

Figure 14

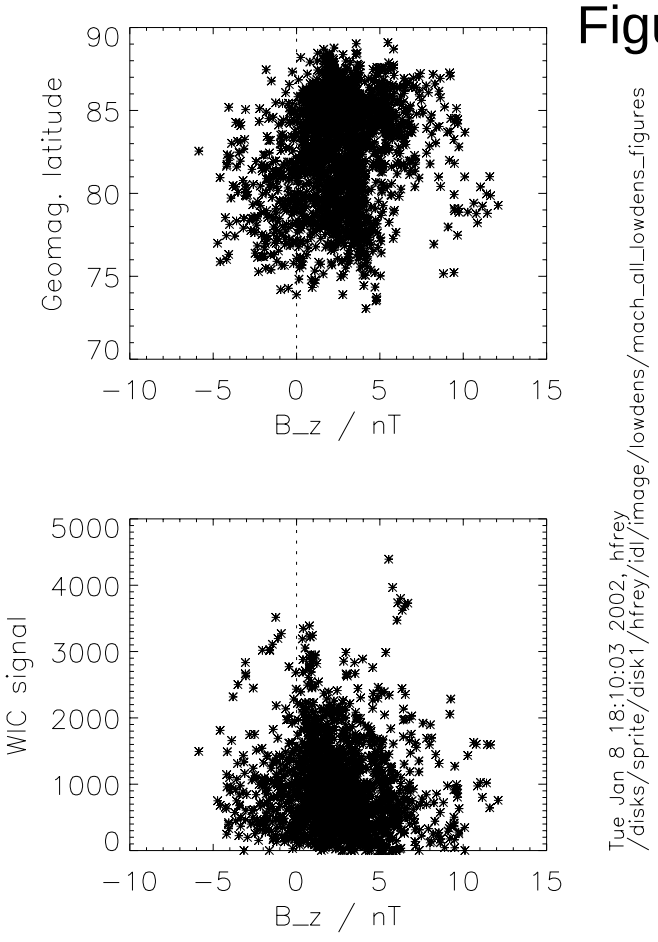
Geomag. latitude
90
85
80
75
70
−10
−5
0
5
10
15
B_z / nT
WIC signal
5000
4000
3000
2000
1000
0
−10
−5
0
5
10
15
B_z / nT
Tue Jan 8 18:10:03 2002, hfrey
/disks/sprite/disk1/hfrey/idl/image/lowdens/mach_all_lowdens_figures

Figure 15

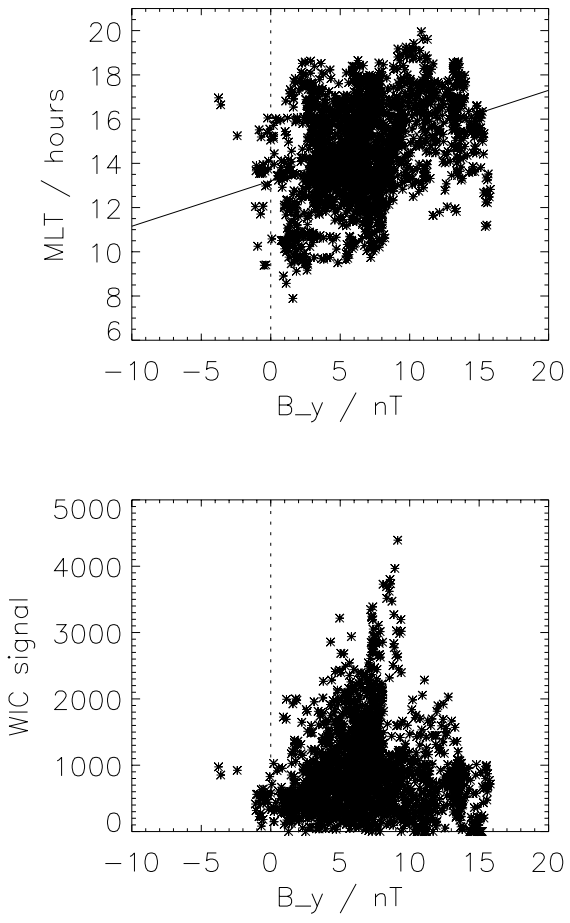
MLT / hours
B_y / nT
WIC signal
B_y / nT
Tue Jan 8 18:04:46 2002, hfrey
/disks/sprite/disk1/hfrey/idl/image/lowdens/mach_all_lowdens_figures

Figure 16

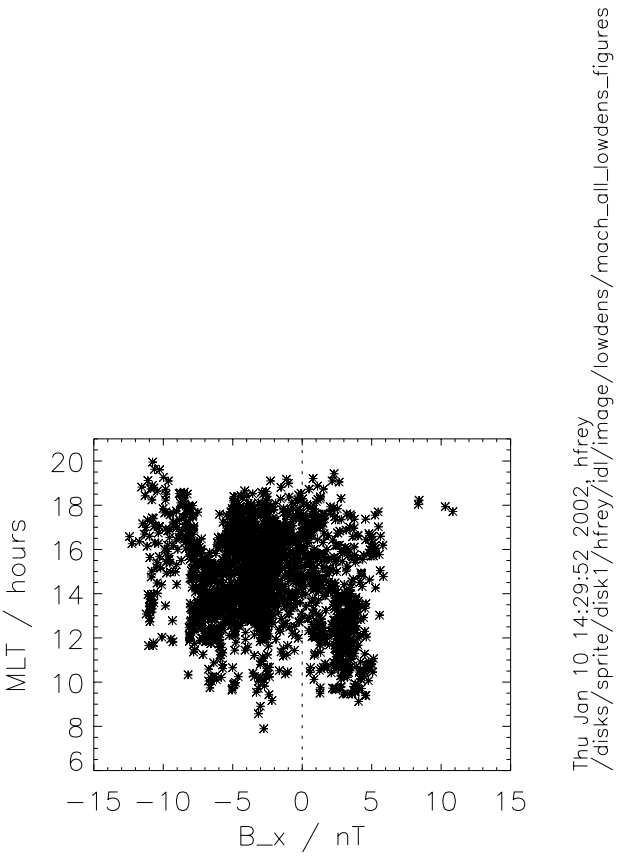
MLT / hours
20
18
16
14
12
10
8
6
−15 −10 −5 0 5 10 15
B_x / nT
Thu Jan 10 14:29:52 2002, hfrey
/disks/sprite/disk1/hfrey/idl/image/lowdens/mach_all_lowdens_figures

Figure 17

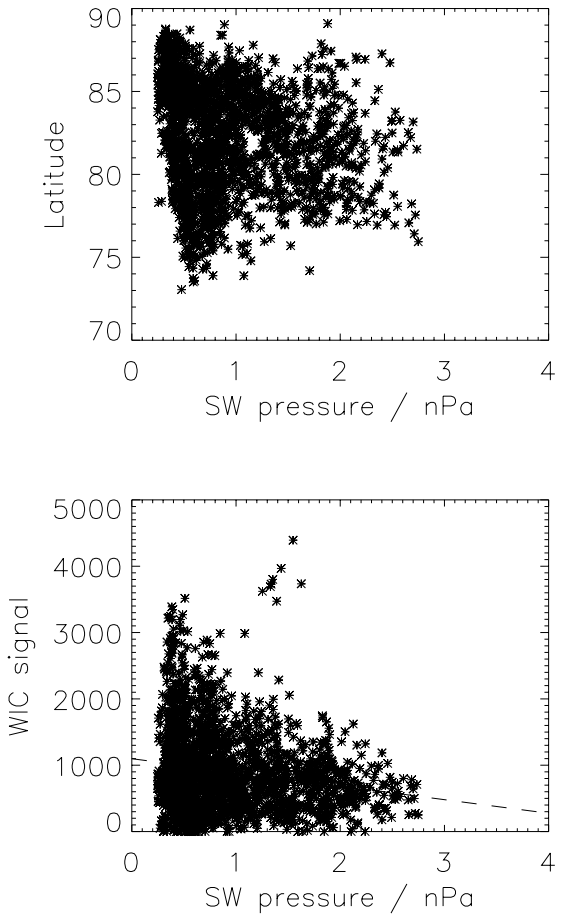
90
85
80
75
70
Latitude
0
1
2
3
4
SW pressure / nPa
5000
4000
3000
2000
1000
0
WIC signal
0
1
2
3
4
SW pressure / nPa
Tue Jan 8 18:07:35 2002, hfrey
/disks/sprite/disk1/hfrey/idl/image/lowdens/mach_all_lowdens_figures

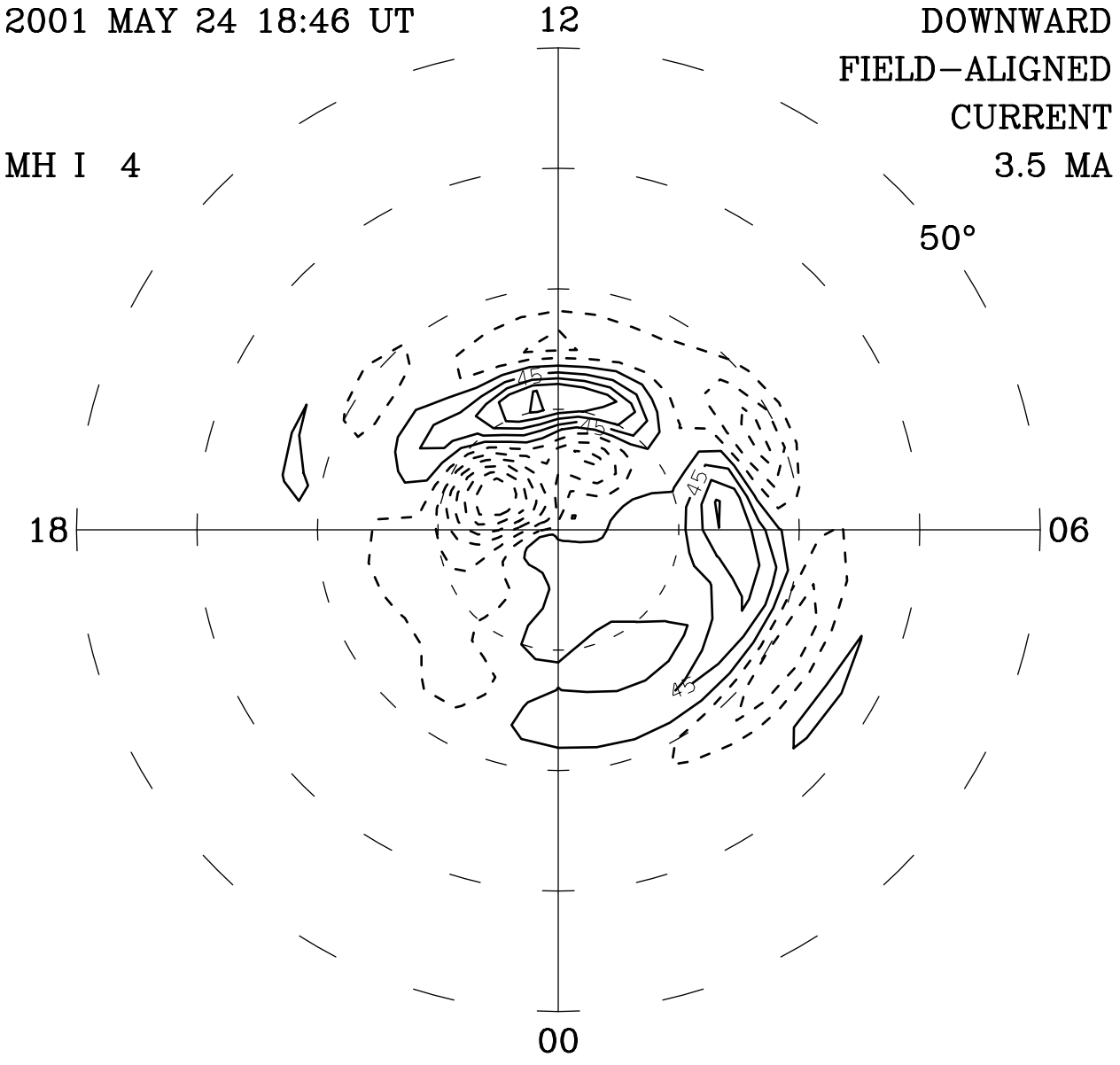

02/04/02 (FITTED)

CONTOUR FROM -0.76500E-05 TO 0.40500E-05 CONTOUR INTERVAL OF 0.30000E-06 PT(3,3)= 0.36138E-06 LABELS SCALED BY 0.10000E+09